Current control loop design and analysis based on resonant regulators for microgrid applications

Federico, de Bosio; Pastorelli, Michelle; de Sousa Ribeiro, Luiz Antonio ; Soares Lima, Marcel; Freijedo Fernandez, Francisco Daniel; Guerrero, Josep M.

Published in:
Proceedings of the IEEE Industrial Electronics Conference 2015

DOI (link to publication from Publisher):
10.1109/IECON.2015.7392938

Publication date:
2015

Document Version
Early version, also known as pre-print

Current control loop design and analysis based on resonant regulators for microgrid applications

F. de Bosio, M. Pastorelli
Energy Department
Politecnico di Torino
Torino, Italy

L. A.de S. Ribeiro, M. S. Lima
Institute of Electrical Energy
Federal University of Maranhao
Sao Luis MA, Brazil

F. Freijedo, J. M. Guerrero
Department of Energy Technology
Aalborg University
Aalborg, Denmark

***Abstract*— Voltage and current control loops play an important role in the performance of microgrids employing power electronics voltage source inverters. Correct design of feedback loops is essential for the proper operation of these systems. This paper analyzes the influence of state feedback cross-coupling in the design of resonant regulators for inner current loops in power converters operating in standalone microgrids. It is also demonstrated that the effect of state feedback cross-coupling degrades the performance of the control loops by increasing the steady-state error. Different resonant regulators structures are analyzed and compared, performing experimental tests to validate the results of the theoretical analysis.**

Keywords—voltage and current regulators; proportional+resonant (PR), complex vector PR

I. INTRODUCTION

Voltage and current regulators are fundamental in modern applications of power electronics, such as variable speed drives, active power filters, and microgrids [1],[2],[3]. The converter employed for these purposes is the Voltage Source Inverter (VSI), following the specific application it can be controlled operating in the current or voltage control mode. The inner loops are responsible for controlling current/torque in AC machines, harmonic compensation in active power filters and microgrids, and voltage regulation in isolated microgrids. Hence, accurate control of current, voltage or both is required for the VSI to succeed in implementing the desired feature of each application. It is expected from any current or voltage regulator to [3],[4]: *i*) provide zero steady-state error; *ii*) accurately track the commanded reference during transients; *iii*) bandwidth as higher as possible; and *iv*) decrease or minimize the total harmonic distortion.

Although nonlinear current regulators such as hysteresis controllers can achieve these challenge goals, secondary effects as variable switching frequency are undesirable in several applications. Furthermore, due to its nonlinear nature, basic control tools cannot be applied in the analysis and design of these regulators. On the other hand, linear regulators suit very well for analysis with classical control theory. Among linear controllers the synchronous reference frame proportional integral (PI) [4], and proportional resonant (PR) [5] are the most common regulators used in these applications. Due to the importance of these controllers, there has been substantial research activity in the subject throughout the years [6-9].

The classical synchronous frame PI regulators work with dc quantities having zero steady-state error. However, they need rotational transformations to rotate the measured quantities to the d-q rotating frame and the commanded output back to the stationary frame. This can be a drawback when implemented in low cost general purpose digital signal processor due to the computation of the transformations. PR controllers do not require these rotations and can be used in single-phase systems. The PR controller [5] is derived from two synchronous frame PI regulators [4], one for the positive sequence and the other for the negative sequence component of the signal, but it is implemented in the stationary reference frame. In some applications, non-ideal PR is used to avoid implementation problems in low cost processors. Another resonant controller, called complex vector PR was initially applied in sensorless AC drives [10]. It is derived from two complex vector PIs [11] and is implemented in the stationary reference frame.

This paper investigates different current control implementations based on resonant controllers for VSI connected in isolated microgrids. Even though extensive research has been done in systems with a strong electromotive force (emf), the isolated microgrid structure has not been completely analyzed. In islanded microgrids the coupling between the capacitor voltage and inductor current has a strong influence in the performance of PR regulators. Thus, the aim of this paper is to analyze the performance of PR regulators, the effect of voltage coupling in the performance of these regulators, and the fundamental differences between the PR controllers.

II. SYSTEM DESCRIPTION

The control of parallel-connected VSIs in isolated microgrids is based on droop control strategy that provides the voltage and frequency references for the inner loops [3]. The inner current and voltage loops are cascaded and, in general, are tuned using serial tuning. The bandwidth of the inner current loop is set to the maximum value allowed by the system stability, in order to increase the dynamic performances and reduce the interactions with the voltage loop. The reduction of the interactions between the current and voltage loops move to a more robust design.

In isolated microgrids the VSI operates in voltage mode where the capacitor voltage and inductor currents are the controlled quantities. The general block diagram of the system including a three-phase inverter with its respective control loops is presented in Fig. 1. With reference to Fig. 1, the voltage and current are measured and transformed to the stationary reference frame ($\alpha\beta$) being $\boldsymbol{i}_{\alpha\beta} = i_\alpha + j i_\beta$,

$\boldsymbol{v}_{\alpha\beta} = v_\alpha + jv_\beta$ the inductor current and capacitor voltage vectors, respectively.

The voltage loop, with the limitations imposed by its bandwidth, controls the converter output voltage by fixing the current reference. The inner current loop controls the inverter states in order to follow the current reference.

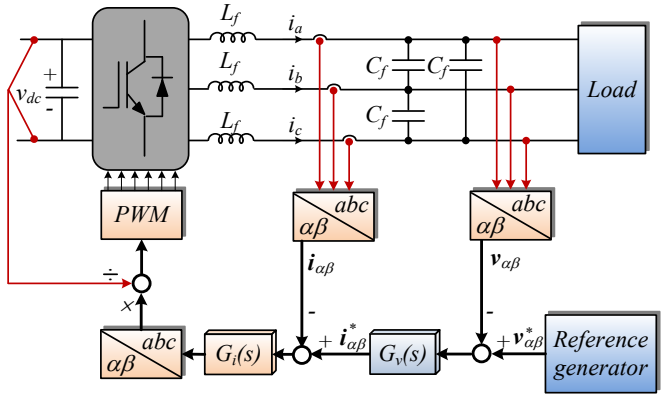

Fig. 1. Block diagram of a three phase VSI with voltage and current loops

The simplified control block diagram of the closed-loop system is shown in Fig. 2, where $\boldsymbol{v}^*_{\alpha\beta}$ and $\boldsymbol{i}^*_{\alpha\beta}$ are the reference voltage and current vectors, $\boldsymbol{i}_{o\alpha\beta}$ is the output current vector, L_f is the filter inductor, R_f is the equivalent series resistance of the inductor, and C_f is the filter capacitor value. $G_i(s)$ and $G_v(s)$ are respectively the current and voltage regulators transfer functions, and $G_{pwm}(s) = [1 - (T_d/2)s]/[1 + (T_d/2)s]$ is the transfer function related to computation and PWM delays.

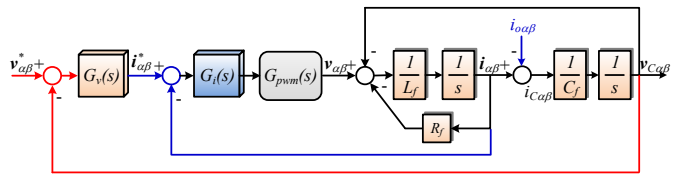

Fig. 2. Simplified block diagram of the closed-loop system

The design of the controllers is based on the serial tuning which means that initially the innermost loop must be tuned. In this case the current loop must be tuned firstly using the block diagram of Fig. 3.

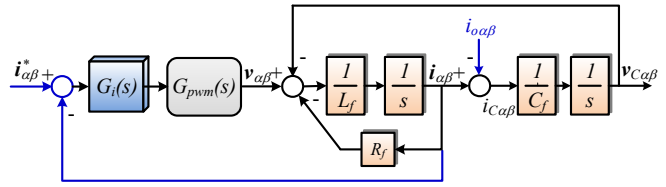

Fig. 3. Block diagram for the design of the current regulator

The current regulators analyzed in this work are: *i*) ideal PR; *ii*) non-ideal PR, and *iii*) complex vector PR. The transfer functions of each regulator are presented in TABLE I. , where k_{pI} and k_{iI} are the proportional and integral gains, while $\omega_o = 2\pi 50$ rad/s is the fundamental resonant frequency, and h is the harmonic order of the resonant frequency to be compensated.

The general approach to design this loop is to neglect the capacitor cross-coupling that can be treated as a disturbance. This is the basic assumption in AC drives and grid connection application, as the emf is strong, and acts as disturbance to the current regulator. If this approach is used in the system of Fig. 3 the closed-loop transfer function is (1).

TABLE I. INNER CURRENT LOOP CONTROLLERS

Non-ideal PR controller	Ideal PR controller	Complex vector PR controller
$k_{pI} + \frac{2\omega_c k_{iI} s}{s^2 + 2\omega_c s + (h\omega_o)^2}$	$k_{pI} + \frac{k_{iI} s}{s^2 + (h\omega_o)^2}$	$\frac{k_{pI} s^2 + k_{iI} s}{s^2 + (h\omega_o)^2}$

$$i_{\alpha\beta}(s) = \frac{G_i(s)G_{PWM}(s)}{L_f s + R_f + G_i(s)G_{PWM}(s)} i^*_{\alpha\beta}(s) - \frac{1}{L_f s + R_f + G_i(s)G_{PWM}(s)} v_{C\alpha\beta}(s) \quad (1)$$

The design of the gains for a PR controller can be made starting from the design of a PI regulator employed in the *dq*-synchronous reference frame, since PR regulators are just implementations of two PI controllers in the stationary reference frame. The current regulator was tuned by selecting a controller zero approximately equal to the break frequency of the *RL* load, i.e., $k_{iI}/k_{pI} \cong R_f/L_f$. The controller gain was selected to achieve the desired bandwidth (f_{bw}). By neglecting the delay of the system, the regulator gains can be calculated by using (2). For the delay of the system $T_d = 1.5T_s = 150\ \mu s$, a bandwidth of $1\ kHz$, and the system parameters used (see TABLE II. , these gains are approximately $k_{pI} = 11.32$ and $k_{iI} = 628$.

$$k_{pI} = 2\pi \mathrm{f_{bw}} L_f\ ; \qquad k_{iI} \cong \frac{R_f}{L_f} k_{pI} \qquad (2)$$

However, when the delay model is considered, the regulator gains for the same bandwidth are presented in TABLE III. For the value of the delay used in this application, and the bandwidth chosen for the inner loop ($f_{bw} = 1\ kHz$), the gain difference neglecting the delay model or including it is more than 50%.

TABLE II. SYSTEM PARAMETERS

Parameter	Symbol	Value
Line to line voltage	v_{gll}	400 V
Fundamental frequency	f_g	50 Hz
Rated power	P_{nom}	2.2 kW
Rated current	i_{snom}	3.33 A
Switching frequency	f_{sw}	10 kHz
Sampling period	T_s	100 µs
Filter inductance	L_f	1.8 mH
Filter capacitance	C_f	27 µF
Inductor ESR	R_f	0.1 Ω
Rated load resistance	R_l	68 Ω

TABLE III. CONTROL PARAMETERS

Parameter	Symbol	Value
Proportional gain	k_{pI}	5.61
Integral gain	k_{iI}	311
Damping term	ω_c	5 rad/s

III. Frequency Response Analysis Without Voltage Decoupling

Because of the cross-coupling between the capacitor voltage and inductor current the formula (1) is not adequate to analyze the system, specifically for the closed loop pole locations. The system presented in (1) with the controllers, and the parameters of TABLE II. and TABLE III. is a 4th order system that is stable for the anlyzed controllers.

The relationship between the states variables is presented in (4). Substituting (4) into (1) it yields to the transfer function (5). This is a 5th order transfer function that results in an unstable system when the complex vector PR is used, independently of the regulator gains. Therefore, it is more appropriate to analyze the system performance.

$$v_{C\alpha\beta}(s) = \left[i_{\alpha\beta}(s) - i_{o\alpha\beta}(s)\right] \frac{1}{C_f s} \qquad (3)$$

The frequency response (FR) for each regulator was analyzed for different values of integrator gain k_{iI} in the range from 11 to 511 to see its effect on the closed loop system. This range was chosen in order to have values around the one that produces zero-pole cancelation ($k_{iI} = 311$). The effect of the disturbance was not analyzed since the main goal of the inner current loop is to track the command, while the outer voltage loop is responsible for disturbance rejection.

Fig. 4 shows the closed loop FR of the system showed in Fig. 3 using the non-ideal PR as current regulator. It can be observed that:

1) The controller ability to produce zero steady-state error at the desired frequency (50 Hz) is affected by the integrator gain (k_{iI}), the smaller its value the bigger will be the error at 50 Hz;
2) Variations of the resonant frequency (reference of the regulator), while the resonant gain ω_o is kept constant at the tuned resonant frequency, can lead to a significant impact in the steady-state error, especially if the parameter ω_c is small;

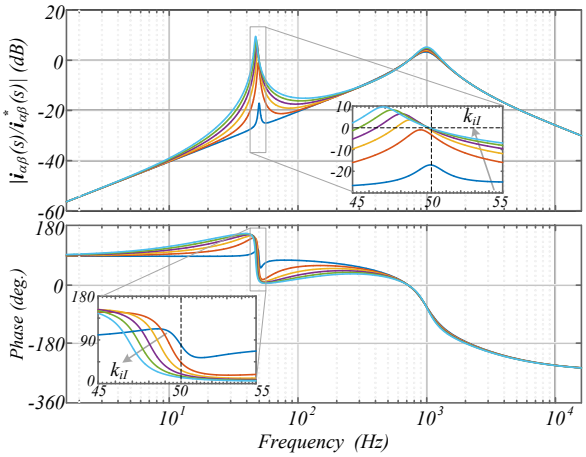

Fig. 4. Closed loop FR of the inner current loop with non-ideal PR regulator and without voltage decoupling: $k_{pI} = 5.61$; $k_{iI} = 11 - 511$ (arrows indicate increasing of k_{iI}).

Fig. 5 shows the closed loop FR when the ideal PR is used in the system of Fig. 3. It can be observed that:

1) The regulator is able to produce zero steady-state error at the desired line frequency (50 Hz);
2) The system FR is very sensitive to frequency variations (reference of the regulator) around the fundamental frequency. Small changes in the reference regulator frequency, while the resonant gain ω_o is kept constant at the tuned resonant frequency, can result in very high steady-state error;
3) Low integrator gain (k_{iI}) values increase the sensitivity to frequency variations.

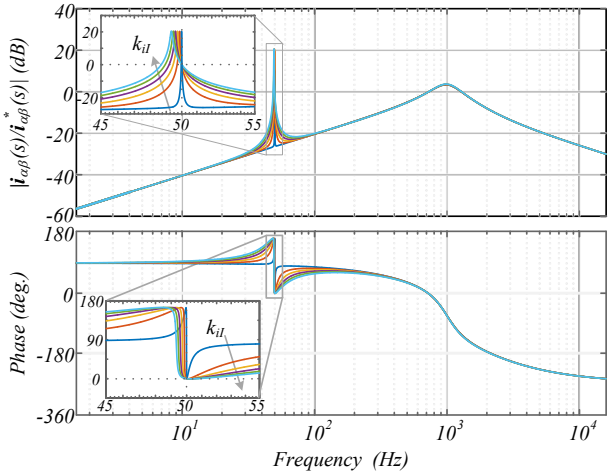

Fig. 5. Closed loop FR of the inner current loop with ideal PR regulator and without voltage decoupling: $k_{pI} = 5.61$; $k_{iI} = 11 - 511$ (arrows indicate increasing of k_{iI}).

The fundamental reason why the ideal PR has an overshoot around the resonant frequency can be explained based on the behavior of a PI regulator in the synchronous reference frame. As said before, PR regulators are based on the implementation of two PI controllers. For the simple case of a PI controller and an RL load the complex vector block diagram is shown in Fig. 6. As shown in [11] the nature of the controller zero and plant pole are different, one real (k_i/k_p) and the other complex ($-R/L - j\omega_e$).

This mismatch is a function of the synchronous frequency and, for a given bandwidth, it results in closed loop dominant poles close to imaginary axis that produce overshoot in the response. As also shown in Fig. 6 this behavior can be overcome decoupling the cross-coupling due to the synchronous reference frame implementation. The PR regulator is the implementation of two of these controllers in the stationary reference frame, as shown in Fig. 7(a). As can be seen in Fig. 7(b).the cross-coupling decoupling of the positive sequence regulator cancels the decoupling of the negative sequence regulator. Therefore, the problem that is present in the synchronous frame PI when there is no decoupling is also present in the PR regulator no matter if a decoupling is done.

$$i_{\alpha\beta}(s) = \frac{G_i(s)G_{PWM}(s)C_f s}{L_f C_f s^2 + R_f C_f s + G_i(s)G_{PWM}(s)C_f s + 1} i^*_{\alpha\beta}(s) + \frac{1}{L_f C_f s^2 + R_f C_f s + G_i(s)G_{PWM}(s)C_f s + 1} i_{o\alpha\beta}(s) \quad (4)$$

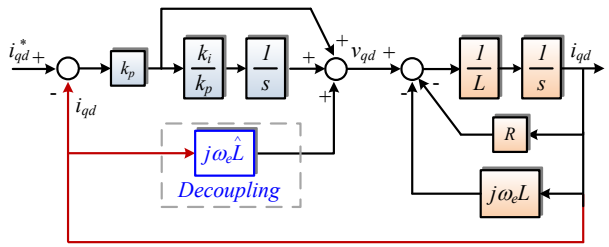

Fig. 6. Closed loop complex vector block diagram of an *RL* load with a synchronous frame, shown in synchronous reference frame (ω_e)

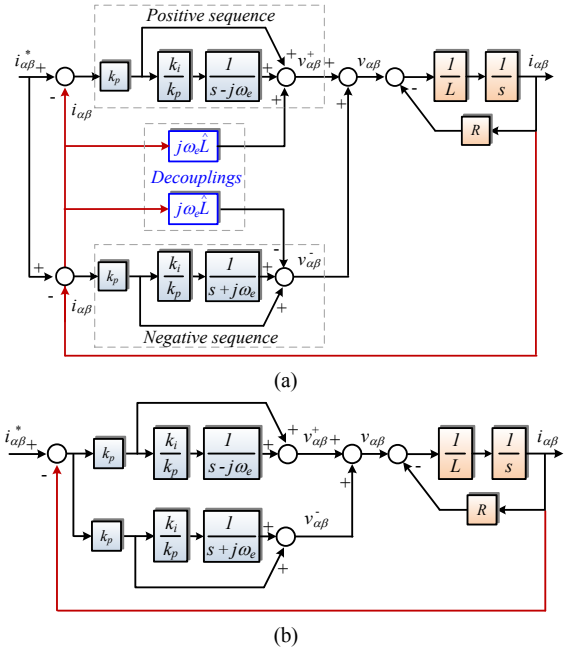

Fig. 7. PR regulator with an RL load: (a) expliciting show the decoupling; (b) resulting regulator

The complex vector root locus for two different synchronous frequencies, with the current regulator tuned to cancel the pole plant ($k_i/k_p = R/L$), is shown in Fig. 8. At low resonant frequencies (Fig. 8a), the controller zero Z_c (a complex number) approximately interact more with the controller pole P_c (also a complex number), both being close to the plant poles P_p. As the controller`s bandwidth increases the closer the zero and closed loop poles will be. This allows the response of the system to be dominated by the faster closed-loop pole. Furthermore, less oscillation is expected since the closed loop poles are moving away from the imaginary axis.

As the resonant frequency increases (for the same bandwidth) the resulting slower closed loop roots become closer to the imaginary axis and away from the zero. Therefore, more oscillation is expected. The results become worse as the resonant frequency increases, and the regulator bandwidth decreases. This can be a serious problem when harmonic compensators are used since these regulators are supposed to work at high resonant frequencies, and, in general, have low bandwidth.

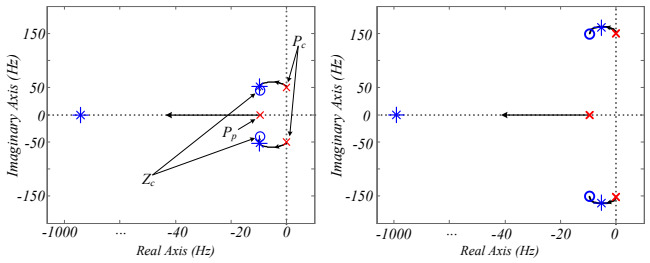

Fig. 8. Complex vector root locus of RL load with PR regulator: x – open loop poles; * closed loop poles; o – zeros (a) resonant frequency 50 Hz; (b) resonant frequency 150 Hz.

Although the complex vector PR is not suited for use with the system of Fig. 3 due to instability it is worth to analyze its closed loop FR. Fig. 9 shows its FR for the same bandwidth and variation of k_{iI}. It can be observed that:

1) The controller is able to produce zero steady-state error at the resonant frequency (50 Hz);
2) The system response has low sensitivity to frequency variations around the resonant frequency. This feature is well suited for systems whose frequency changes;
3) Changes in the integrator gain (k_{iI}) have almost any influence in the FR around the resonant frequency, at least in the range observed. This feature is basically due to closer zero and pole design of this controller.

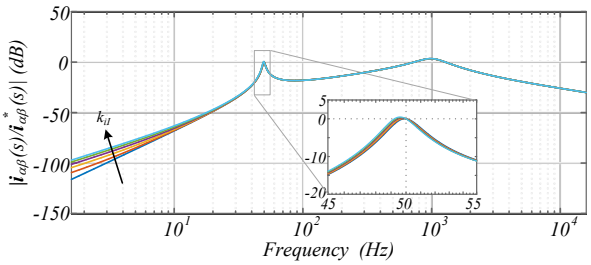

Fig. 9. Closed loop FR of the inner current loop with complex vector PR regulator and without voltage decoupling: $k_{pI} = 5.6$; $k_{iI} = 11 - 511$ (arrows indicate increasing of k_{iI}).

If it is possible to stabilize the system showed in Fig. 3 the complex vector PR regulator would be the right choice due to its interesting features, especially with the frequency changes which is normally the case in droop controlled microgrids.

The reason why the system (Fig. 3) is unstable is due to the capacitor voltage cross-coupling. Therefore, if a voltage decoupling is performed the complex vector PR can be used and the system can take advantage of its good properties.

IV. Frequency Response Analysis With Voltage Decoupling

If the output voltage is measured, it is possible to decouple its effect on the inner current loop. Fig. 10 shows this design. By considering ideal voltage cross-coupling decoupling (in practice a lead compensator must be included to compensate for the PWM transfer function delay), the closed loop transfer function is just the first term of (1). The load does not disturb the current regulator anymore.

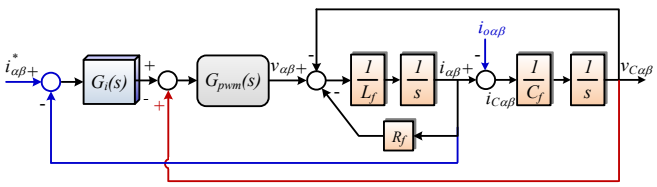

Fig. 10. Block diagram of the inner current loop with output voltage cross-coupling decoupling

For the FR showed in this section the controllers parameters were the same as in the previous section. Fig. 11 shows the closed loop FR of non-ideal PR controller with output voltage cross-coupling decoupling. It can be observed that:

1) The controller is able to produce zero steady-state error at the desired fundamental frequency (50 Hz), depending on the value of k_{iI};
2) The smaller the integrator gain (k_{iI}) the bigger will be the error at 50 Hz. However, the error is very small and is fundamentally in the phase;
3) The system FR has low sensitivity to frequency variations around the resonant frequency. However, the smaller k_{iI} the bigger will be the sensitivity around 50 Hz;
4) The corrective effect of the non-ideal PR controller around the resonant frequency is just 2%;
5) Changes in the resonant frequency have little impact in the steady-state error;
6) The effect of voltage cross-coupling decoupling is more important than the use of the PR controller.

Fig. 12 shows closed loop FR of ideal PR controller with output voltage cross-coupling decoupling. The same conclusions as for the case of ideal PR controller can be drawn, except that in this case the variations are much smaller. Again, the effect of voltage decoupling is significant.

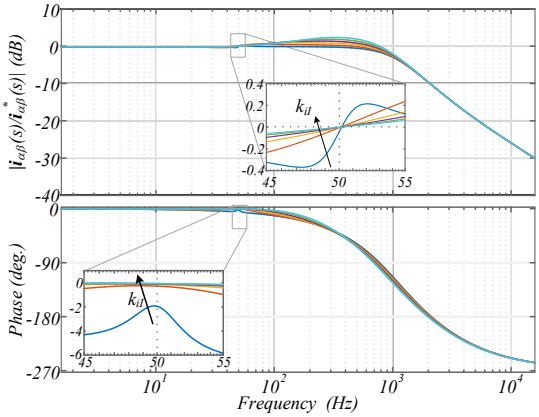

Fig. 11. Closed loop FR of the inner current loop with non-ideal PR regulator, and with voltage decoupling: $k_{pI} = 5.61$; $k_{iI} = 11 - 511$ (arrows indicate increasing of k_{iI}).

Fig. 13 shows the closed loop FR of complex vector PR controller with output voltage cross-coupling decoupling. The same conclusions as for the case of complex vector PR regulator without decoupling are true, thus the errors are extremely low around the resonant frequency. Comparing the complex vector PR regulator with the others analyzed in this paper, it is clear that it shows the lowest sensitivity to frequency variations around the fundamental frequency. Therefore, it is probably the most indicated for use in applications where the resonant frequency changes as in droop controlled microgrids.

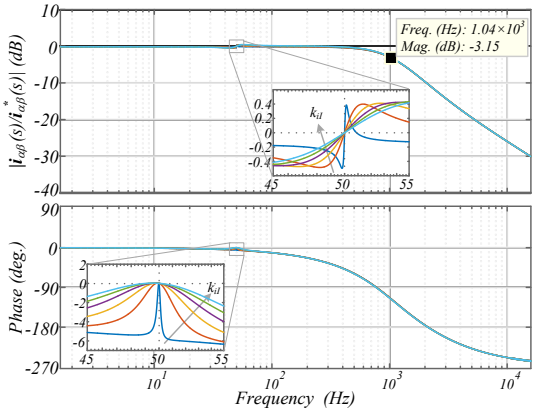

Fig. 12. Closed loop FR of of the inner current loop with ideal PR regulator, and with voltage decoupling: $k_{pI} = 5.61$; $k_{iI} = 11 - 511$ (arrows indicate increasing of k_{iI}).

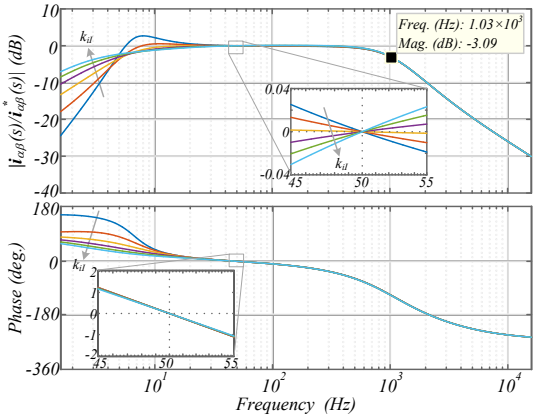

Fig. 13. Closed loop FR of of the inner current loop with complex vector PR regulator, and with voltage decoupling: $k_{pI} = 5.61$; $k_{iI} = 11 - 511$ (arrows indicate increasing of k_{iI}).

V. Experimental Results

The power system of Fig. 1 was tested in the laboratory to validate the analysis presented in the previous sections. For this purpose, a 2.2 kVA power converter, driven by dSpace DS1006 platform, has been employed. The proportional and integral gains and the load impedance values are reported in TABLE II. and TABLE III. The regulators were implemented in discrete time using forward and backward Euler discretization of the two cascaded integrators used in the PRs regulators. The analysis are performed without and with capacitor voltage decoupling.

As expected from the FR analysis all the three controllers produce approximately zero steady-state error when designed to have exactly the same resonant frequency as the one of the reference current, and with sufficient high k_{iI} as the one presented in Table III.

To analyze the sensitivity of the PR regulators to frequency variations the reference current frequency was changed to 49 Hz, while the resonant frequency of the

regulators was kept constant in 50 Hz. Fig. 14 and Fig. 15 show the steady-state currents and errors for ideal and non-ideal PR regulators without and with voltage decoupling. It is clear that the effect of voltage decoupling has a significant impact on the performance of the closed loop system, reducing significantly the error. Furthermore, the sensitivity of the ideal PR to frequency variations is bigger than the sensitivity of the non-ideal PR. For this last regulator the zero steady-state error with voltage decoupling depends on the value of k_{iI}. Fig. 16 shows an experimental result for the non-ideal PR with $k_{iI} = 11$. For small values of this gain, the regulator does not provide zero steady-state error, even with voltage decoupling.

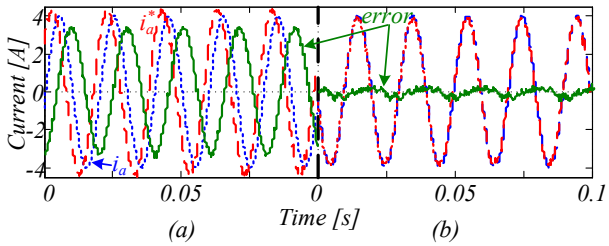

Fig. 14. Steady-state currents and error for ideal PR: (a) without voltage decoupling; (b) with voltage decoupling -$f_{ref} = 49\ Hz$, $k_{iI} = 311$

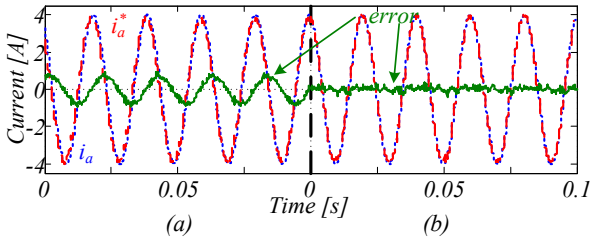

Fig. 15. Steady-state currents and error for non-ideal PR: (a) without voltage decoupling; (b) with voltage decoupling -$f_{ref} = 49\ Hz$, $k_{iI} = 311$

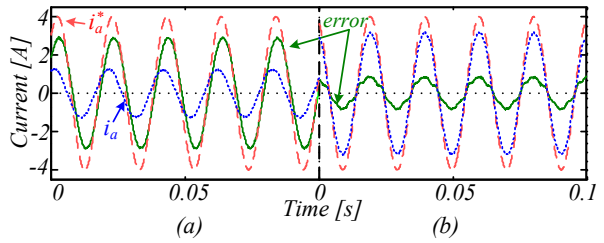

Fig. 16. Steady-state currents and error for non-ideal PR: (a) without voltage decoupling; (b) with voltage decoupling -$f_{ref} = 49\ Hz$, $k_{iI} = 11$

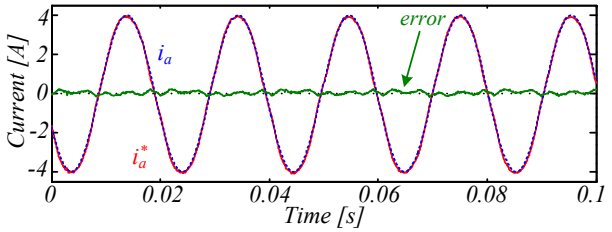

Fig. 17. Steady-state currents and error for Compex vector PR with voltage decoupling - $f_{ref} = 49\ Hz$, $k_{iI} = 11$:

Fig. 17 shows the results for the complex vector PR. This controller produces zero steady-state error even for small values of k_{iI}.

VI. Conclusions

This paper shows the design and a detailed analysis of the inner current loop for power converters, based on resonant controllers. The benefits of applying capacitor voltage decoupling are evidenced by the lower steady-state error and independence from the load impedance.

Complex vector PR controller, which is stable only if voltage decoupling is performed, shows the lowest sensitivity to integral gain and frequency deviation, thus it can be preferred in microgrid applications.

Acknowledgment

The authors would like to thanks the motivation and support provided by CNPq/Brazil, CEMAR and University of Aalborg.

References

[1] D. G. Holmes, T. A. Lipo, B. P. McGrath, and W. Y. Kong, "Optimized Design of Stationary Frame Three Phase AC Current Regulators," *Power Electronics, IEEE Transactions on,* vol. 24, pp. 2417-2426, 2009.

[2] C. Lascu, L. Asiminoaei, I. Boldea, and F. Blaabjerg, "High Performance Current Controller for Selective Harmonic Compensation in Active Power Filters," *Power Electronics, IEEE Transactions on,* vol. 22, pp. 1826-1835, 2007.

[3] J. C. Vasquez, J. M. Guerrero, M. Savaghebi, J. Eloy-Garcia, and R. Teodorescu, "Modeling, Analysis, and Design of Stationary-Reference-Frame Droop-Controlled Parallel Three-Phase Voltage Source Inverters," *Industrial Electronics, IEEE Transactions on,* vol. 60, pp. 1271-1280, 2013.

[4] T. M. Rowan and R. J. Kerkman, "A New Synchronous Current Regulator and an Analysis of Current-Regulated PWM Inverters," *Industry Applications, IEEE Transactions on,* vol. IA-22, pp. 678-690, 1986.

[5] D. N. Zmood and D. G. Holmes, "Stationary frame current regulation of PWM inverters with zero steady-state error," *Power Electronics, IEEE Transactions on,* vol. 18, pp. 814-822, 2003.

[6] K. Hongrae, M. W. Degner, J. M. Guerrero, F. Briz, and R. D. Lorenz, "Discrete-Time Current Regulator Design for AC Machine Drives," *Industry Applications, IEEE Transactions on,* vol. 46, pp. 1425-1435, 2010.

[7] J. Holtz, Q. Juntao, J. Pontt, J. Rodriguez, P. Newman, and H. Miranda, "Design of fast and robust current regulators for high-power drives based on complex state variables," *Industry Applications, IEEE Transactions on,* vol. 40, pp. 1388-1397, 2004.

[8] A. G. Yepes, F. D. Freijedo, J. Doval-Gandoy, Lo, x, O. pez, *et al.*, "Effects of Discretization Methods on the Performance of Resonant Controllers," *Power Electronics, IEEE Transactions on,* vol. 25, pp. 1692-1712, 2010.

[9] A. G. Yepes, F. D. Freijedo, O. Lopez, and J. Doval-Gandoy, "Analysis and Design of Resonant Current Controllers for Voltage-Source Converters by Means of Nyquist Diagrams and Sensitivity Function," *Industrial Electronics, IEEE Transactions on,* vol. 58, pp. 5231-5250, 2011.

[10] L. A. S. Ribeiro, M. W. Degner, F. Briz, and R. D. Lorenz, "Comparison of carrier signal voltage and current injection for the estimation of flux angle or rotor position," in *Industry Applications Conference, 1998. Thirty-Third IAS Annual Meeting. The 1998 IEEE*, 1998, pp. 452-459 vol.1.

[11] F. Briz, M. W. Degner, and R. D. Lorenz, "Analysis and design of current regulators using complex vectors," *Industry Applications, IEEE Transactions on,* vol. 36, pp. 817-825, 2000.